

Hubble Diagram Dispersion From Large-Scale Structure

Timothy Clifton^{*} and Joe Zuntz

Oxford Astrophysics, Physics, DWB, Keble Road, Oxford, OX1 3RH, UK

In original form 2009 February 4

ABSTRACT

We consider the effects of large structures in the Universe on the Hubble diagram. This problem is treated non-linearly by considering a Swiss Cheese model of the Universe in which under-dense voids are represented as negatively curved regions of space-time. Exact solutions for luminosity distances and redshifts are derived, and used to investigate the non-linear effects of structure on the magnitudes of astrophysical sources. It is found that intervening voids, between the observer and source, have no noticeable effect, while sources inside voids can be effected considerably. By averaging observable quantities over many randomly generated distributions of voids we find that the presence of these structures has the effect of displacing the average magnitude from its background value, and introducing a dispersion around that average. Observers in an inhomogeneous universe, who take averages of observables along many different lines of sight, may then introduce systematic biases, and under-estimate errors, if these effects are not taken into account. Estimates of the potential size of these effects are made using data from the Millennium Simulation.

Key words: cosmology: theory – relativity – large scale structure of Universe – supernovae: general – cosmological parameters

1 INTRODUCTION

Hubble diagrams play a key role in our understanding of the evolution of the Universe. It was Hubble diagrams that first led to widespread acknowledgement of the expanding Universe paradigm, and today, in the form of type Ia supernova observations, they provide important evidence for the Dark Energy that is at the heart of the Λ CDM model of the Universe. Ongoing and future projects aim to collect more and more data in order to reconstruct the expansion history of the Universe to ever increasing accuracy, and to test hypotheses about the nature of Dark Energy itself.

Given the extraordinary implications of the supernova results, and the large amounts of resources that are being invested in them, it seems prudent to make sure we fully understand all physical effects that may bias, or influence, the conclusions which are drawn from them. To this end, we perform a detailed, and fully non-linear, investigation of the effects of the simplest large structures on Hubble diagrams.

That structure exists on small scales in the Universe is, of course, indisputable, but while some studies of galaxy surveys have pointed toward homogeneity on scales of ~ 30 Mpc (Hogg et al. 2005), others have concluded that the largest structures so far detected are limited only by the size of the surveys that found them (Labini et al. 2008). The apparent recent detection of an anomalously large local bulk flow

(Watkins, Feldman & Hudson 2008), as well as the existence of unexpected features in the CMB (Land & Magueijo 2005; Inoue & Silk 2006), and the CMB dipole itself, also hint at the possibility of large structures existing in the Universe. Here we do not wish to debate the evidence for or against structure existing on different scales, but rather to calculate the effects that different structures have on Hubble diagrams.

The majority of studies in this area have been performed within the context of linear perturbation theory (Dyer & Roeder 1972, 1973, 1974; Sasaki 1987; Futamase & Sasaki 1989; Kasai, Futamase & Takahara 1990; Kantowski 1998; Sugiyama, Sugiyama & Sasaki 1999; Pyne & Birkinshaw 2004; Bonvin, Durrer & Alice Gasparini 2006). Here we treat the problem non-perturbatively by modelling the Universe as a Friedmann-Robertson-Walker (FRW) background, with spherical sections removed and replaced by regions of Lemaitre-Tolman-Bondi (LTB) space-time (Lemaître 1933; Tolman 1934; Bondi 1947). With an appropriate choice of boundary conditions between the FRW and LTB regions, the resulting geometry is an exact solution of Einstein’s equations. Such a solution is often referred to as a Swiss Cheese universe, although the replaced regions here are not completely empty.

The Swiss Cheese approach has a number of drawbacks, but its great benefit is that it allows calculations to be performed beyond the linear level. As the solution is exact,

^{*} E-mail: tclifton@astro.ox.ac.uk

and as it is possible to derive simple expressions for redshift and luminosity distances within it, all higher order and non-perturbative effects are automatically included. Luminosity distances in Swiss Cheese universes have been studied previously by Biswas & Notari (2008) and Marra et al. (2007), who were both interested in investigating whether or not Dark Energy could be made redundant in these more general models. Our goal here is not to construct a situation in which one can fit for the observations without Dark Energy, but rather to attempt to calculate the effect of inhomogeneities on Hubble diagrams for the purposes of better understanding their influence on parameter estimation, or, conversely, on constraining structure, if cosmological parameters are deemed to be known from elsewhere. Our results differ from those presented by Biswas & Notari (2008), and are concerned with considerably less extreme circumstances than those of Marra et al. (2007).

In section 2 we introduce the theory. We will briefly discuss the LTB solution, and how it can be embedded into an FRW universe. We then go on to a more detailed discussion of redshifts and luminosity distances in the resulting space-time. This is done by considering bundles of null geodesics, and the Sachs optical equations. We provide a rigorous derivation of the commonly used distance measures for source- and observer-centric space-times, and generalise to the case of both source and observer off centre. The results presented in this section are new, but the reader more interested in astrophysical consequences can skip this section without damaging the comprehensibility of later sections.

In section 3 we investigate the effect of a single large void in the Universe on luminosity distances as functions of redshift. Measures of distance to objects on the other side of the void appear largely unaffected by its presence. Observations of objects that reside inside the void, however, can be considerably affected by the void's presence. We present results for the change in luminosity distance that can result from voids of varying depths, widths and at different redshifts. Results here are limited to the case of looking through the centre of voids, but could be generalised in a straightforward, if computationally more intensive, way.

Section 4 contains an analysis of the effect of looking through many voids in a row. In this section the voids are drawn from idealised distributions. Examples are presented, and the case of averaging over many lines of sight is analysed. Such averaging of luminosity distances, for specified geometries, appears to us to be a preferable, if more cumbersome method, than averaging the mass distribution, and calculating a single luminosity distance in the corresponding geometry. We present results for the dispersion, and deviation, of Hubble diagrams that results from different distributions of voids.

In section 5 we make an attempt at linking the idealised cosmologies, considered in previous sections, to some more realistic distributions of matter. We take density profiles generated from linear perturbations about a uniform background, and from the Millennium Simulation. These profiles are produced by a process of averaging over different length scales. The profiles are then idealised, so as to fit into the framework developed in the preceding sections, and the results on Hubble diagrams are calculated.

Finally, in section 6, we conclude.

2 SWISS CHEESE COSMOLOGY

The cosmology we consider here is an FRW background with spherical regions removed and replaced with LTB space-times, in order to model inhomogeneities. Sub-sections 2.1-2.3 recap standard results on LTB space-times. Sub-section 2.4 then contains a derivation of new results on luminosity distances in these space-times, for both observer and source away from the centre of symmetry.

2.1 The LTB Solution

The LTB line-element is given by (Lemaître 1933; Tolman 1934; Bondi 1947)

$$ds^2 = -dt^2 + \frac{R'^2}{(1 - kr^2)} dr^2 + R^2 d\Omega^2, \quad (1)$$

where $R = R(t, r)$, $k = k(r)$ and prime denotes partial differentiation with respect to r . For $\Lambda = 0$ and $k < 0$ we can write R in parametric form as

$$R = \frac{m(1 - \cosh \Theta)}{2kr^2} \quad (2)$$

$$t - t_0 = \frac{m(\sinh 2\Theta - 2\Theta)}{2(-kr^2)^{3/2}} \quad (3)$$

where $t_0 = t_0(r)$ and $m = m(r)$. Exact solutions exist for $\Lambda \neq 0$, and are given in terms of elliptic functions by Zecca (1991). It is also possible to solve for the case with $k \geq 0$, but this will not be required here. The geometry (1) is an exact solution of Einstein's equations in the presence of a perfect fluid of pressureless dust with energy density

$$\rho = \frac{m'}{R^2 R'}. \quad (4)$$

Gauge freedoms allow us to transform into a coordinate system in which $t_0 = \text{constant}$, without loss of generality. The LTB space-time is then completely specified by a choice of $k(r)$ and $m(r)$, and reduces to FRW in the limit $k(r) = \text{constant}$. We will refer to $k(r)$ as the spatial curvature and $m(r)$ as the gravitational mass distribution.

2.2 Boundary Conditions

We now wish to replace regions of FRW with the LTB geometry described above. To do this we need the conditions required to match a manifold with metric (1) to one with FRW metric

$$ds^2 = -dt^2 + a^2(t) (dx^2 + f^2(x) d\Omega^2) \quad (5)$$

at a boundary of constant $r = x = \Sigma$. The Darmois junction conditions imply that the matching is a solution of Einstein's equations if the first and second fundamental form on the hyper-surface at Σ are identical on either side (Bonnor & Vickers 1981). This corresponds to the two conditions (Ribeiro 1992)

$$R|_{\Sigma} = af|_{\Sigma} \quad (6)$$

$$\sqrt{1 - kr^2}|_{\Sigma} = f'|_{\Sigma}, \quad (7)$$

which can be verified to describe the requirement that the LTB metric should reduce to FRW at the boundary.

2.3 Null Geodesics and Redshifts

Now consider a null geodesic in (1) with affine parameter λ , and with a tangent vector $k^a = dx^a/d\lambda$. If n^a is the unit vector in the direction of k^a , in the rest space of an observer with 4-velocity u^a , then k^a can be decomposed as

$$k^a = (-u_b k^b)(u^a + n^a), \quad (8)$$

where $u_a u^a = -1$, $n_a n^a = 1$ and $u_a n^a = 0$. Thus, for a radial null geodesic, and an observer co-moving with the coordinate system (1), we have $u^a = (1, 0, 0, 0)$ and $n^a = (0, \pm\sqrt{1-kr^2}/R', 0, 0)$. The \pm sign here corresponds to geodesics directed away, or toward, the centre of symmetry, and we have chosen λ to increase with t . According to (8), an infinitesimal increment in affine parameter, $d\lambda$, will then be seen by the observer following u^a as changes in time and position of

$$dt = -u_a k^a d\lambda \quad (9)$$

$$dr = \mp u_a k^a \frac{\sqrt{1-kr^2}}{R'} d\lambda. \quad (10)$$

This agrees with the equation for radial null geodesics, which can be read off from (1) as

$$\frac{dr}{dt} = \pm \frac{\sqrt{1-kr^2}}{R'}. \quad (11)$$

The tangent vectors for radial geodesics can now be written as $k^a = (A, B, 0, 0)$, where $A = A(t, r)$ and $B = B(t, r)$. The trajectories to which k^a are tangent are both null and geodesic, so that $k^a k_a = 0$ and $k^a k^b{}_{;a} = 0$. This gives $B = \pm A\sqrt{1-kr^2}/R'$, and

$$k^a = A \left(1, \pm \frac{\sqrt{1-kr^2}}{R'}, 0, 0 \right), \quad (12)$$

where A as the solution of

$$\pm \sqrt{1-kr^2} A' + \dot{A} R' + A \dot{R}' = \frac{dA}{dt} R' + A \dot{R}' = 0. \quad (13)$$

This expression integrates to

$$A \propto \exp \left\{ - \int \frac{\dot{R}'}{R'} dt \right\}. \quad (14)$$

As always, the redshift of a photon is given by

$$1+z = \frac{(u^a k_a)_e}{(u^b k_b)_o}, \quad (15)$$

where subscript e denotes a quantity at the point where the photon is emitted, and subscript o a quantity at the point it is observed. In the present situation we have $u^a k_a = -A$, so the redshift is

$$1+z = \frac{A_e}{A_o} = \exp \left\{ \int_e^o \frac{\dot{R}'}{R'} dt \right\}, \quad (16)$$

in agreement with the source centred case considered by Bondi (1947), and the observer centric case considered by Ribeiro (1992). This expression is valid for any source and observer connected by a radial geodesic, be they centred or not.

2.4 Luminosity Distances

Consider a bundle of null geodesics with cross-sectional area $d\sigma$, and tangent vector k^a . The rate of change of $d\sigma$ along the bundle is

$$\frac{d(d\sigma)}{d\lambda} = k^a{}_{;a} d\sigma, \quad (17)$$

and is independent of the 4-velocity of the screen onto which it is projected (Sachs 1961).

First let us consider an observer at the centre of symmetry. In this case, we wish to know the cross-sectional area of a bundle of null geodesics focused on the origin. The expansion scalar of the field of tangent vectors to the radial geodesics (12) in the space-time (1) is given by

$$k^a{}_{;a} = 2 \frac{A}{R} \left(\dot{R} \pm \sqrt{1-kr^2} \right), \quad (18)$$

where use has been made of (13). Equation (17) then gives

$$d(\ln d\sigma) = 2 \frac{A}{R} \left(\dot{R} \pm \sqrt{1-kr^2} \right) d\lambda \quad (19)$$

$$= 2 \frac{\dot{R}}{R} dt + 2 \frac{R'}{R} dr \quad (20)$$

$$= 2d(\ln R), \quad (21)$$

where in going to the second line we have used (9) and (10). The equation above then integrates to give

$$d\sigma \propto R^2. \quad (22)$$

This is equivalent to the statement usually read off from the line-element (1) directly, that the angular diameter distance for an observer at the centre of an LTB space-time is

$$r_A^2 \equiv \frac{d\sigma}{d\Omega} = R^2(t_e, r_e). \quad (23)$$

The angular diameter distance can be related to the galactic angular distance, r_G , by Etherington's theorem (Etherington 1933), so that

$$r_G^2 = (1+z)^2 R^2(t_e, r_e), \quad (24)$$

which gives the luminosity distance, r_L , as

$$r_L^2 = (1+z)^4 R^2(t_e, r_e), \quad (25)$$

where the factors of $(1+z)$ are given by (16). These expressions reduce to the usual FRW ones in the appropriate limits.

Now consider an observer away from the centre of symmetry. In order to determine the angular diameter distance they measure, we want to be able to find the cross-sectional area of a bundle of null geodesics focused on a point away from the centre of symmetry, and centred about a radial geodesic pointing toward the centre of symmetry. This can be achieved using equation (17), once a suitable field of tangent vectors to such a bundle, \hat{k}^a , is found. To do this we first transform from spherical polar to Cartesian coordinates, $(r, \theta, \phi) \rightarrow (x, y, z)$, using the usual transformations. We then shift $x \rightarrow \hat{x} - x_0$, and transform back to spherical coordinates, $(\hat{x}, y, z) \rightarrow (\hat{r}, \hat{\theta}, \hat{\phi})$, using the inverse transformations. The resulting line-element can be straightforwardly computed, but is lengthy, and so will not be displayed here.

The field of tangent vectors, \hat{k}^a , to the bundle focused at $\hat{r} = 0$ (i.e. $r = x_0$) can now be found by solving the geodesic equations $\hat{k}^a \hat{k}^b{}_{;a} = 0$, together with the null condition $\hat{k}^a \hat{k}_a = 0$, and imposing the additional constraint $\hat{k}^{\hat{\theta}} = \hat{k}^{\hat{\phi}} = 0$ as $\hat{r} \rightarrow 0$. Here this task is simplified as we are interested in the cross-sectional area of a bundle of rays centred around the vector pointing from $\hat{r} = 0$ to $r = 0$, where $\hat{k}^{\hat{\theta}}$ and $\hat{k}^{\hat{\phi}}$ must

equal 0 anyway, due to symmetry. Along this trajectory, the null condition then gives

$$\hat{k}^a = \hat{A} \left(1, \pm \frac{\sqrt{1 - k(\hat{r} - x_0)^2}}{R'}, 0, 0 \right), \quad (26)$$

which is identical to (12), with r replaced by $\hat{r} - x_0$. This is as expected, as it is simply the vector connecting the points $\hat{r} = 0$ and $r = 0$.

We can now use (17), and the results above, to find the cross-sectional area of the bundle focused at $\hat{r} = 0$ to be

$$\begin{aligned} & \frac{d(\ln d\hat{\sigma})}{d\hat{\lambda}} \\ &= 2\hat{A} \left(\frac{\dot{R}}{R} \pm \frac{\sqrt{1 - k(\hat{r} - x_0)^2}}{R} \pm \frac{x_0 \sqrt{1 - k(\hat{r} - x_0)^2}}{\hat{r}(x_0 - \hat{r})R'} \right). \end{aligned} \quad (27)$$

As (26) is the same as (12), up to a replacement of r with $\hat{r} - x_0$, we therefore also have that dt and $d\hat{r}$ are given by (9) and (10), with r replaced by $\hat{r} - x_0$, and where primes now refer to partial derivatives with respect to \hat{r} . Using these relations (27) can be written as

$$d(\ln d\hat{\sigma}) = 2\frac{\dot{R}}{R}dt + 2\frac{R'}{R}d\hat{r} + \frac{2x_0}{\hat{r}(x_0 - \hat{r})}d\hat{r}, \quad (28)$$

which can be integrated to

$$d\hat{\sigma} \propto \frac{\hat{r}^2 R^2}{(\hat{r} - x_0)^2}. \quad (29)$$

This result has $d\hat{\sigma} = 0$ at $\hat{r} = 0$, showing that the rays are indeed focused at that point. Transforming back to the (t, r, θ, ϕ) coordinates the expression above becomes

$$d\hat{\sigma} \propto \frac{(r_o - r_e)^2 R_e^2}{r_e^2}. \quad (30)$$

Again, this expression reduces to the usual FRW one in the appropriate limit, and also reduces to the expression for an on-centre observer, (23), as $r_o \rightarrow 0$. From Etherington's theorem we know that as $r_e \rightarrow 0$ we have

$$\frac{d\hat{\sigma}}{d\Omega} = \frac{R_o^2}{(1+z)^2}. \quad (31)$$

It is known that for LTB space-times to be non-singular at the origin it must be the case that as $r \rightarrow 0$, we have $R/r \rightarrow \text{constant}$, $k \rightarrow \text{constant}$ and $m \rightarrow 0$ (Bonnor 1974). Equation (31) is then compatible with (30) if

$$d\Omega \propto \frac{r_o^2}{A_0^2 R_o^2}. \quad (32)$$

In appendix A we determine the solid angle explicitly, and find it to be consistent with this result. Absorbing constants of proportionality appropriately, and choosing $\hat{\lambda}$ so that $A_0 = 1$, then gives the angular diameter distance between an observer at r_o and an object at r_e as

$$r_A^2 = \frac{(r_o - r_e)^2}{r_o^2 r_e^2} R_o^2 R_e^2. \quad (33)$$

The galactic angular distance, along the same geodesic, is then

$$r_G^2 = \frac{(r_o - r_e)^2}{r_o^2 r_e^2} R_o^2 R_e^2 (1+z)^2, \quad (34)$$

and the luminosity distance is

$$r_L^2 = \frac{(r_o - r_e)^2}{r_o^2 r_e^2} R_o^2 R_e^2 (1+z)^4. \quad (35)$$

This is the required expression for luminosity distance when both observer and source are off-centre. It has the correct limit as either source or observer move to the centre of symmetry, as well as the correct FRW limit¹.

3 A SINGLE VOID

We will now consider the case of a flat FRW Universe containing a single void. We can choose coordinates, without loss of generality, such that $t_0 = \text{constant}$, and so that the big bang occurs simultaneously at all points in space. This condition is automatically satisfied in FRW if surfaces of constant density are chosen to be surfaces of equal time. We also choose initial conditions such that $m \propto r^3$, so that the gravitational mass is initially evenly distributed. The form of the void is then specified by the function $k(r)$, which we will take to be a Gaussian of the form

$$k = k_0 \exp \left\{ - \left(\frac{r}{r_0} \right)^2 \right\}, \quad (36)$$

where $k_0 < 0$ and $r_0 > 0$ are constants specifying the depth and width of the void, respectively. This negative perturbation in k causes the space inside the void to expand faster than that outside, so that the energy density inside the void is dissipated more rapidly. An under-density then occurs, not due to any decrease in gravitational mass, but due to an increase in spatial volume. Although the choices above appear reasonably natural, one may consider more general space-times, either by changing the functional form of $m(r)$ and $k(r)$, or by considering less symmetric space-times than that of LTB. We will postpone considering the effects of such generalisations here, so that we can first concentrate on the simple case of a Gaussian perturbation in curvature outlined above.

3.1 An Einstein-de Sitter background

Consider the case of a void in a space-time that is asymptotically a spatially flat Einstein-de Sitter (EdS) universe, as $r \rightarrow \infty$ in (1). In this case $\Lambda = 0$, and the metric functional $R(t, r)$ is given parametrically by equations (2) and (3). The functions $t = t(z)$ and $r = r(z)$, along past null geodesics, can then be found by integrating equations (11) and (16). Substituting these expressions into equation (35) gives $r_L(z)$. Here we will use this result to investigate the effects such structures have on Hubble diagrams, when observers look through them.

We begin by considering the effect of voids with varying width and depth, at the same position. For ease of computation we consider the space-time as an LTB under-density matched to an FRW background under the conditions (6) and (7), at 3σ from the centre of the void². The geodesic

¹ We note that this expression is different to that obtained by Biswas & Notari (2008), and the process used by Marra et al. (2007).

² Although the Gaussian $k(r)$ is not exactly constant at this point, it has reached $\sim 99\%$ of its asymptotic value, and so is effectively constant.

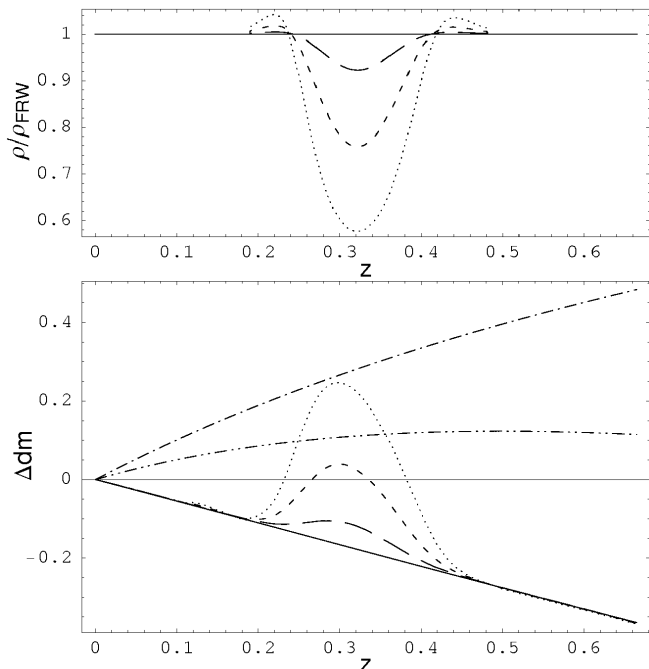


Figure 1. The upper panel shows the fractional energy density experienced by the photon, where the long-dashed, short-dashed and dotted lines correspond to voids that are 10%, 30% and 50% under-dense today. The lower panel shows how these three voids effect the distance modulus. The solid, dot-dashed and double-dot-dashed lines in this plot correspond to EdS, dS and Λ CDM with $\Omega_\Lambda = 0.7$, respectively. These results are with an EdS background.

equations, and redshift relations, must then be integrated in each space-time and $r(z)$ and $t(z)$ matched at the boundaries. The cumulative redshift, $1 + z_T$, is given in the usual way by the expression

$$(1 + z_T) = \prod_i (1 + z_i),$$

where $1 + z_i$ is the redshift along a portion, i , of the geodesic.

The effects of three voids with different depths, all approximately the same width and located at the same redshift $z \sim 0.3$, are shown in Figure 1. The upper plot shows the energy density encountered by a photon as it travels through the three different voids, and the lower plot shows the corresponding distance modulus, Δdm , as a function of redshift, z . Distance modulus is defined as the magnitude an object appears at, minus the magnitude it would have at the same redshift in a empty, negatively curved Milne universe. It can be written in terms of luminosity distance as

$$\Delta dm = 5 \log_{10} r_L - 5 \log_{10} r_L^m, \quad (37)$$

where r_L is given by (35), and $r_L^m = z + z^2/2$ is the expansion normalised luminosity distance in a Milne universe. Anything below $\Delta dm = 0$ in Figure 1 is then interpreted as a decelerating universe, and anything above it as accelerating. For reference, we have included in this plot the distance moduli for an EdS universe, as the solid line, and for a de Sitter (dS) space, as the dot-dashed line.

It can be seen from the upper plot of Figure 1 that, although the spatial curvature k is always negative, the energy density can reach values in excess of the asymptotic value at

the edge of the void. This is due to the analogue of the radial scale factor, R'/r , being lower than its asymptotic value in this region, and could be interpreted as matter from near the edge of the void being pulled away from its centre. Aside from these small over-densities, at the edges of the void, it can clearly be seen that the energy density in the centre of the void has been dissipated as a result of the more rapid expansion there, caused by the negative curvature perturbation. The three voids shown in this plot are chosen such that at their centres they are 10%, 30% and 50% under-dense, at the present time. The upper plot shows these regions to be slightly less under-dense than this at their minima, as what is depicted is the energy density experienced by the photon as it passed through them, sometime before the present.

The lower plot in Figure 1 shows that there is no noticeable effect, due to the void, on viewing objects that are beyond it. While the presence of the voids causes a deviation from the EdS background in their vicinity, it can be seen their distance moduli returns to the background value at redshifts beyond. This means that the Hubble diagrams constructed by looking through these structures is largely unaffected by them, unless the objects being observed are inside the voids themselves. If an object is indeed inside a void, then its deviation from the background value can be seen to be considerable for the examples shown here. Clearly these deviations are a function of the void depth, and increase in a proportionate way.

As well as varying the depth of a void, we will also be interested in the effect of varying its width, and its distance from us. This is shown in Figures 2 and 3. In Figure 2 all three example voids are now chosen to have the same depth, so that they are 50% under-dense today, while their width is varied. The deviation from the background distance modulus changes its width accordingly, and as would be expected. We note that the maximum deviation is approximately the same for each of these voids, showing that it is mainly sensitive to the void depth.

In Figure 3 we show the effect of considering voids at different distances from us. We consider three sets of voids, one set that is 10% under-dense today, another that is 30% under-dense, and a third that is 50% under-dense. The upper plot in this figure shows how the maximum depth of void varies with redshift, for each set of voids. As expected, as the centre of the void is moved to greater redshifts, the minimum density experienced by the photon increases. This is due to the depth of voids increasing with time. Here we do not consider voids that are centred at $z < 0.1$, as we are interested in the effect of distant voids, and not the effect of us living in a void, which is considerable in itself (Alexander, Biswas & Notari 2007; Alnes, Amarzguoui & Grøn; Garcia-Bellido & Haugboelle 2008; Clifton, Ferreira & Land 2008; Bolejko & Wyithe 2008). In the lower plot of Figure 3 we show the maximum deviation in distance modulus, from the background value, for each of the three sets of voids. This maximum deviation can again be seen to be proportionate to the maximum depth of void, as experienced by the photon, and shown in the upper plot.

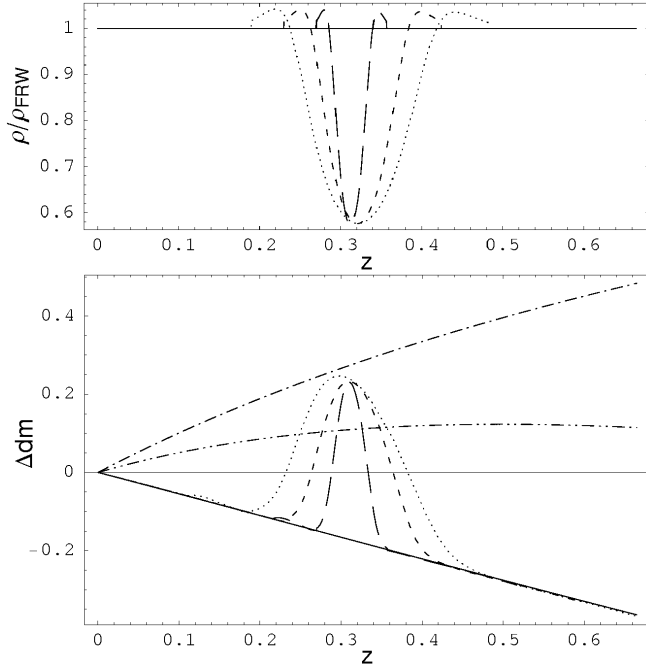


Figure 2. The upper panel shows the fractional energy density for three voids of the same depth, but with varying widths. The lower panel shows the corresponding effect on the distance modulus. Dot-dashed, double-dot-dashed and solid lines are as in Figure 1. These results are with an EdS background.

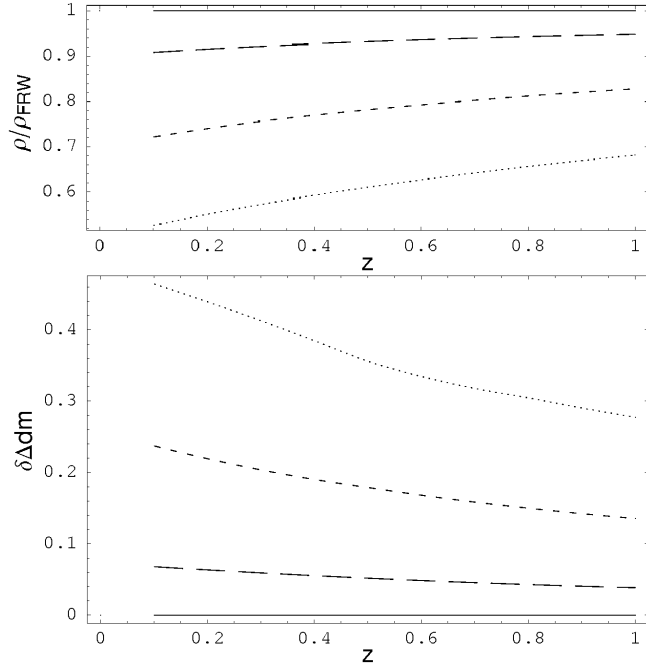


Figure 3. The effect of changing the location of the void. The three voids from Figure 1 are moved to different redshift between $z = 0.1$ and 1 . The upper panel shows how the fractional energy density at the centre of the voids varies with redshift. The lower panel shows the maximum displacement in distance modulus, from the background value, that these voids cause. These results are with an EdS background.

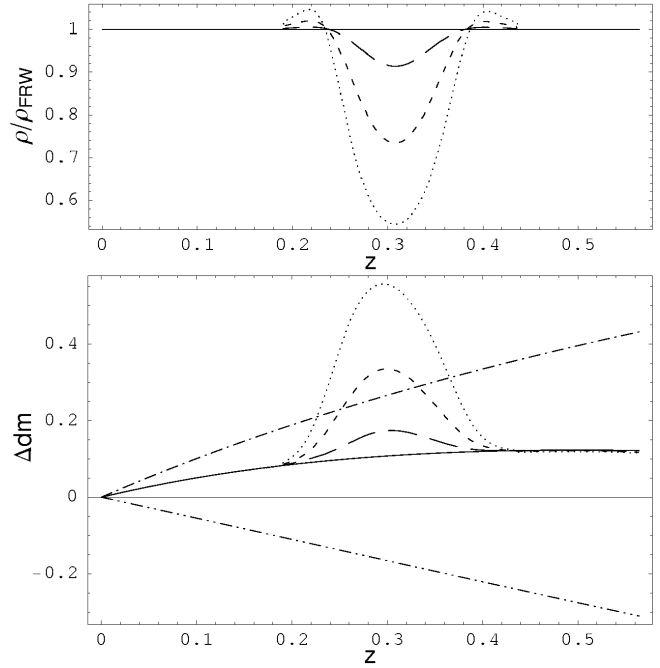


Figure 4. The upper panel is the same as in Figure 1, but the background is now Λ CDM with $\Omega_\Lambda = 0.7$. The lower panel shows the corresponding distance moduli. The solid line in this plot again shows the background, which is now Λ CDM, and the double-dot-dashed line shows EdS.

3.2 A Λ CDM background

As well as a spatially flat, dust dominated EdS background, we are also interested in backgrounds containing a non-zero Λ . To achieve an understanding of this we will repeat the analysis above for the case of a single void in an asymptotically Λ CDM universe with $\Omega_\Lambda = 0.7$ ³. In this case the equations for $r(t)$, $z(t)$ and r_L are unchanged, with the functional form of $R(t, r)$ modified from that given in (2) and (3), in order to include the effects of Λ (Zecca 1991).

Figure 4 shows the same three voids as Figure 1, with under-densities of 10%, 30% and 50% and centred at $z \sim 0.3$. The background is again given by a solid line, but this now corresponds to Λ CDM with $\Omega_\Lambda = 0.7$. The EdS distance modulus is shown by the double-dot-dashed line. The effect of the void can be seen to be largely the same as that shown in Figure 1, when $\Lambda = 0$. The distance modulus returns to that of the background at large z , and there is a displacement from the background value when looking at objects in the void. It can be seen that the energy density experienced by the photon is closer to the value of the under-density today in this case, reflecting the fact that the growth of structure slows when Λ comes to dominate.

Figure 5 illustrates the dependence of the distance modulus on the width of void in this background, and the results can be seen to be very similar to those deduced from Figure 2. The maximum deviation from the background is again most sensitive to the depth of the void, and not its width. In Figure 6 we consider the maximum deviation of the distance modulus from its background value, for the same three sets

³ With radiation neglected, which should be a good approximation in the epochs under consideration.

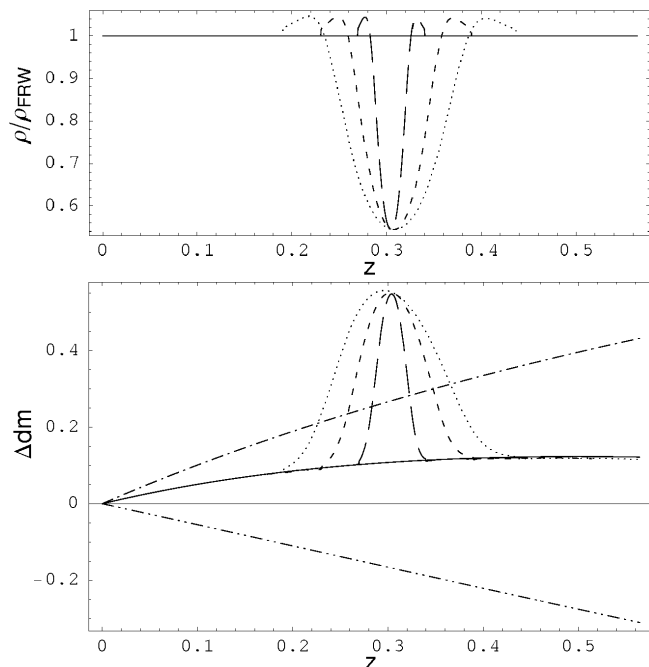


Figure 5. The upper panel is the same as Figure 2, but now with a Λ CDM background with $\Omega_\Lambda = 0.7$. The lower panel shows the corresponding distance moduli, with the solid and double-dot-dashed lines as in Figure 4.

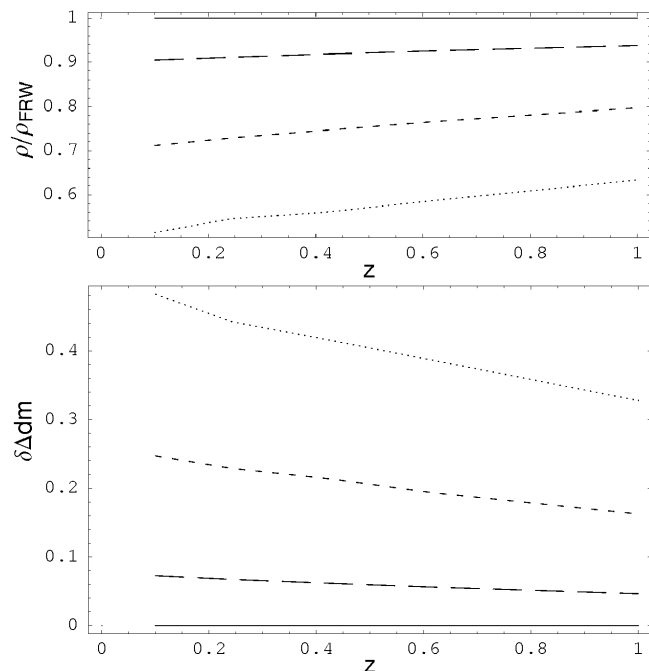


Figure 6. The same as Figure 3, but with a Λ CDM background with $\Omega_\Lambda = 0.7$.

of voids as in Figure 3. The results are remarkably similar to the EdS case, the principle difference appearing to be the weaker dependence of the depth of under-density on z , due to the suppression of structure formation in the presence of Λ . This manifests itself in the lower plot of Figure 6 as a slightly shallower gradient.

4 MANY VOIDS

The effect of a single void on Hubble diagrams is of some interest by itself. Such effects could be used to search for hypothesised large structures, such as that which is supposed to explain the CMB cold spot (Inoue & Silk 2006). However, if we suppose that a single large void exists in the Universe, then it is natural to think that there will be other structure on similar scales. In this section we consider just such a scenario, with many LTB voids lined up back to back in an FRW background.

4.1 An Einstein-de Sitter background

Again, we will first consider the case of a spatially flat EdS background. Now instead of inserting a single void, satisfying the boundary conditions (6) and (7), we will insert a number of voids. As before, we will match these voids to the background cosmology at 3σ from their centre, where they are effectively FRW. The choice of voids that can be used for this process is quite arbitrary. Here we will randomly select voids from a couple of different distributions, in order to gain some understanding. This process can, of course, be repeated for any distribution of voids one may wish to consider.

4.1.1 Distribution A: Shallow voids

For this example we will consider voids with present day depths drawn from a Gaussian distribution that is peaked at 0% under-dense, and has a standard deviation of 10% (i.e. so that $\sim 68\%$ of voids are less than 10% under-dense, and $\sim 95\%$ are less than 20% under-dense). The width of voids will be drawn from a flat probability distribution, and will be between 0.05 and 0.25 redshifts wide when viewed by an observer standing at their edge today. Although these choices allow for the existence of large structures, we do not consider them extreme.

In Figure 7 we show an example set of voids, out to $z = 1$, picked from this distribution. As was the case previously, the upper plot shows the energy density encountered by a photon that reaches us at the present day. We ensure that we are not in a void by placing the edge of the first void at a redshift of $z = 0.05 + w$, where w is a random number between 0 and 0.2 (the reason for introducing w will be made clear shortly). As before, the solid line in the lower plot is the background FRW universe, which here is EdS. The dot-dashed lines and double-dot-dashed lines represent the distance moduli of dS and Λ CDM with $\Omega_\Lambda = 0.7$, respectively. While there are clear deviations from the background distance modulus, it seems highly unlikely that a distribution of voids of this type could be mistaken for Λ CDM with $\Omega_\Lambda = 0.7$.

Having considered an example set of voids, it is now of interest to consider the average of many different sets drawn from the same probability distribution. This may be the type of process that one would wish to consider when collecting observations made over many different lines of sight, at different points on the sky. Such an average is shown in Figure 8. Here 1000 different sets of voids have been generated, their distance moduli calculated, and an average taken. Shown in the plot is the resulting mean deviation from the

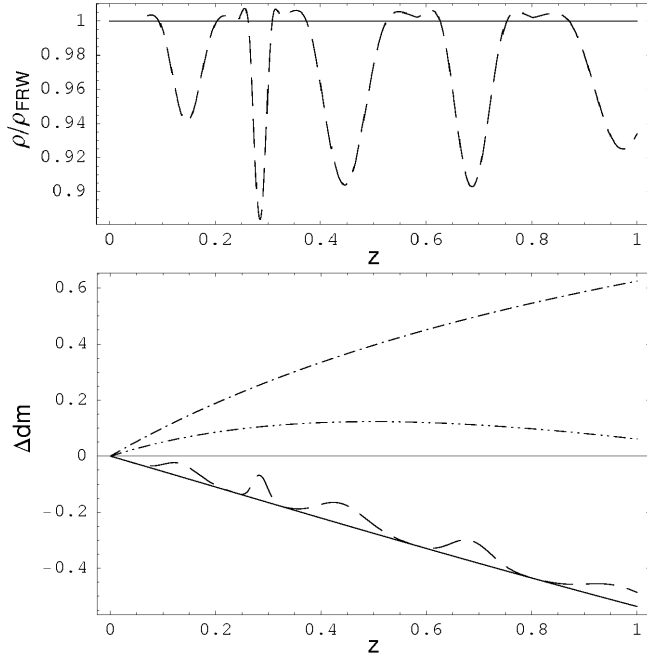


Figure 7. The upper panel shows a sample set of voids taken from the shallow distribution of voids, with $\sim 68\%$ of voids $< 10\%$ under-dense. The lower plot shows the corresponding distance modulus. The dot-dashed, double-dot-dashed and solid lines are as in Figure 1. These results are with an EdS background.

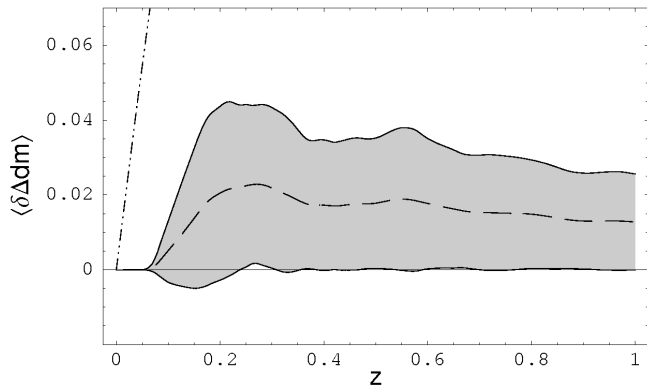


Figure 8. This plot shows the result of averaging the distance moduli of 1000 sets of voids randomly drawn from the shallow distribution, with $\sim 68\%$ of voids $< 10\%$ under-dense. Displayed is the mean deviation from the EdS background, the dashed line, and the standard deviation about that mean, the grey area. Also displayed for reference is the deviation of Λ CDM with $\Omega_\Lambda = 0.7$ from EdS, as the double-dot-dashed line.

background value, the central dashed line, and the standard deviation from this value, the shaded region. The rise at $z = 0.05$ is due to the void free region out to $z = 0.05 + w$. The effect of w here is to make the location of the edge of the first void random (failing to include w leads to a correlation in the location of the first void, and an increased mean at that point).

The effect of looking at objects in an inhomogeneous universe of this kind is two-fold. Firstly, there is a systematic deviation away from the distance modulus of the background. This appears to be reasonably small for the void distributions chosen here, with $\langle \delta \Delta m \rangle \leq 0.02$, but is nonethe-

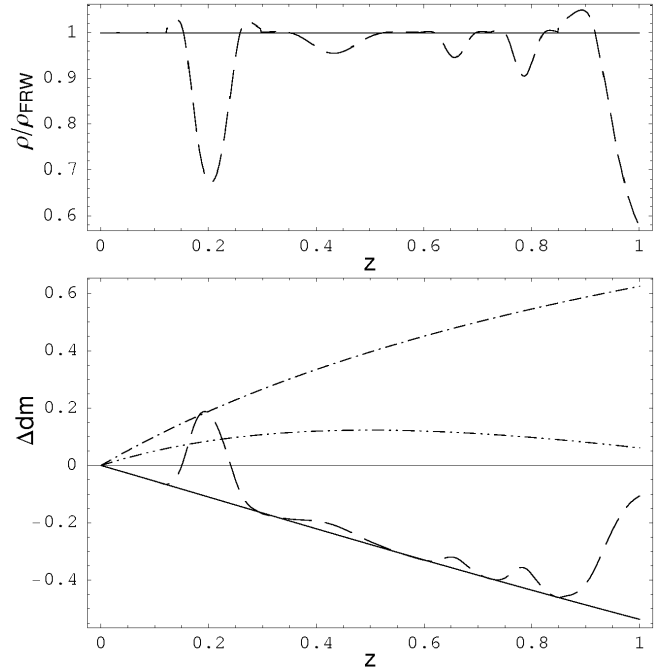


Figure 9. The same as Figure 7, but with voids drawn from the deeper distribution, with $\sim 68\%$ of void $< 25\%$ under-dense.

less non-zero. Such an effect, if unaccounted for, could lead to a systematic bias in extracting cosmological parameters. Secondly, there is a non-zero scatter around the mean. The effect of having a distribution of voids between us and the source should be expected to result in a typical source being somewhat displaced from the mean. Again, the effect caused by this particular distribution of voids are modest, but not zero.

4.1.2 Distribution B: Deeper voids

Having considered one particular distribution of voids, let us now consider a second so that we can better understand the effect of the choice of voids on the resulting averaged distance moduli. From the above considerations of single voids, we know that the maximum displacement of distance modulus is most sensitive to the depth of void. For this reason we will not alter the probability distribution for the width of voids, but instead will modify the distribution from which the depth is drawn. We will keep a Gaussian probability distribution, centred about a 0% under-density, but now will increase the standard deviation of this distribution from 10% to 25% (so that $\sim 68\%$ of voids are less than 25% under-dense at their centre). A sample density profile and distance modulus plot, for voids drawn from this new distribution, is shown in Figure 9. This can be seen to be similar to the results shown in Figure 7, but with the deviations from the background value amplified.

In order to find the mean, and standard deviation, for this new distribution we will proceed as before. 1000 sets of voids are generated, their distance moduli calculated, and then averaged. The results of this are shown in Figure 10. These results are again similar to those obtained from the previous distribution, except with the magnitude of the deviations from the background model being increased in a

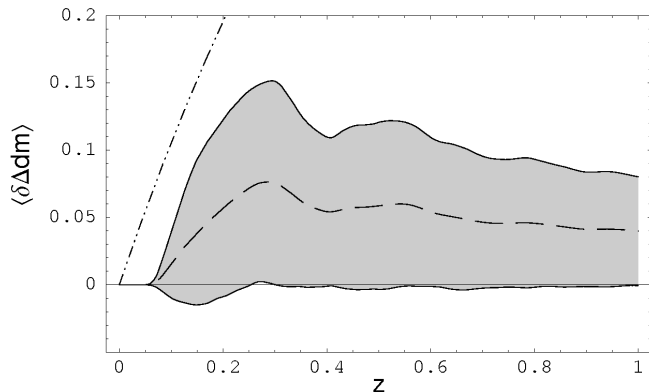


Figure 10. The same as Figure 8, but with voids drawn from the deeper distribution, with $\sim 68\%$ of void $< 25\%$ under-dense.

proportionate way to the increase in void depth. The scatter around the mean is similarly increased.

4.2 Λ CDM background

Having discussed the situation of looking through many voids in an EdS background, we will also be interested in space-times with a non-zero Λ . In this section we will consider a background Λ CDM cosmology with $\Omega_\Lambda = 0.6$. We choose a value for Λ slightly lower than the concordance value in order to illustrate how the effect of voids could lead to incorrect cosmological parameters being extracted from the data, if they are not taken into account. We will take voids from the same two distributions considered above.

4.2.1 Distribution A: Shallow voids

Using the same distribution of shallow voids as above (that is with $\sim 68\%$ of voids with central under-densities $< 10\%$ today), we generate 1000 sets of randomly selected voids. An example set is shown in Figure 11. Here the dotted lines correspond to Λ CDM with $\Omega_\Lambda = 0.6$ today. The concordance value of $\Omega_\Lambda = 0.7$ is shown, for reference, as the double-dot-dashed line. It can be seen that the effect of the voids is to increase the distance modulus. Although this effect is again quite small, it now appears that the dashed line in the lower plot could reasonably be mistaken for a Λ CDM cosmology with a higher value of Ω_Λ , if one were fitting for an FRW cosmology.

In Figure 12 we show the result of averaging over 1000 different sets of randomly generated voids. What is shown here is the deviation from the $\Omega_\Lambda = 0.6$ background value. As before, the central dashed line shows mean deviation, and the shaded region shows the standard deviation from this mean. Included in this plot is a double-dot-dashed line denoting the deviation of the $\Omega_\Lambda = 0.7$ concordance cosmology from the $\Omega_\Lambda = 0.6$ background. These results can be seen to be very similar to those shown in Figure 8, which was for voids drawn from the same distribution, but with $\Lambda = 0$. This is in keeping with the result found in the single void case, that the deviation of the distance modulus, due to the voids, is not particularly sensitive to the value of Λ , except in its effect on suppressing structure formation.

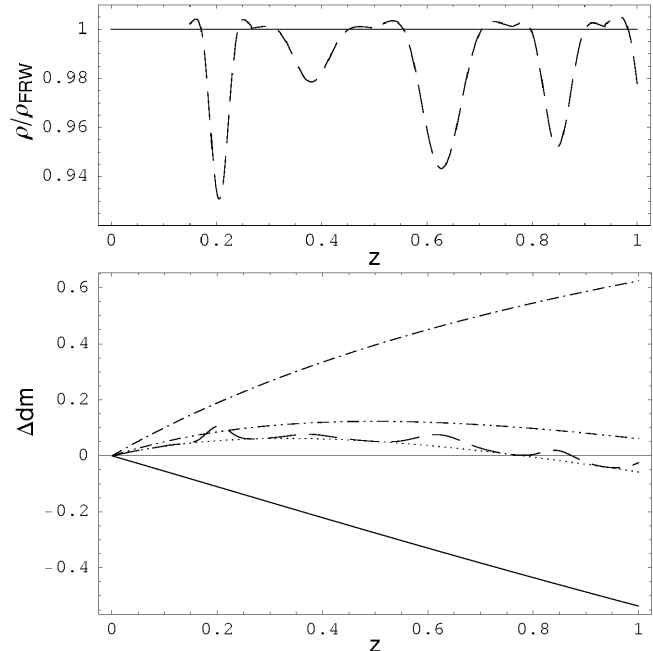


Figure 11. The same as Figure 7, but with a Λ CDM background with $\Omega_\Lambda = 0.6$, shown as the dotted line in the lower panel.

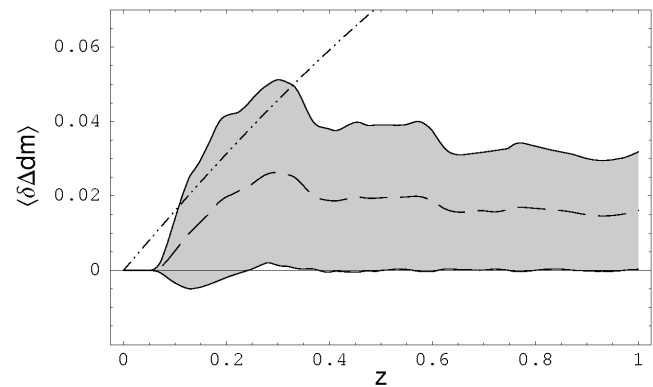


Figure 12. The same as Figure 8, but with a Λ CDM background with $\Omega_\Lambda = 0.6$.

4.2.2 Distribution B: Deeper voids

Finally, let us consider $\Omega_\Lambda = 0.6$ with the distribution of deeper voids, where $\sim 68\%$ of voids are $< 25\%$ under-dense at their centre. An example set of voids, out to $z = 1$, is shown in Figure 13. The effect of these deeper voids is similar to the results found above, but with larger displacements of distance modulus from the background value, as expected.

Figure 14 shows the results of averaging over 1000 sets of voids generated from this distribution. As with the case of shallower voids, the results are similar to those obtained when $\Lambda = 0$, shown in Figure 10.

5 SIMULATED STRUCTURE

In sections 3 and 4 we used exact Swiss Cheese cosmologies to determine the effect of large inhomogeneities on luminosity distances. These situations are of interest as they allow unambiguous, explicit calculations to be performed within

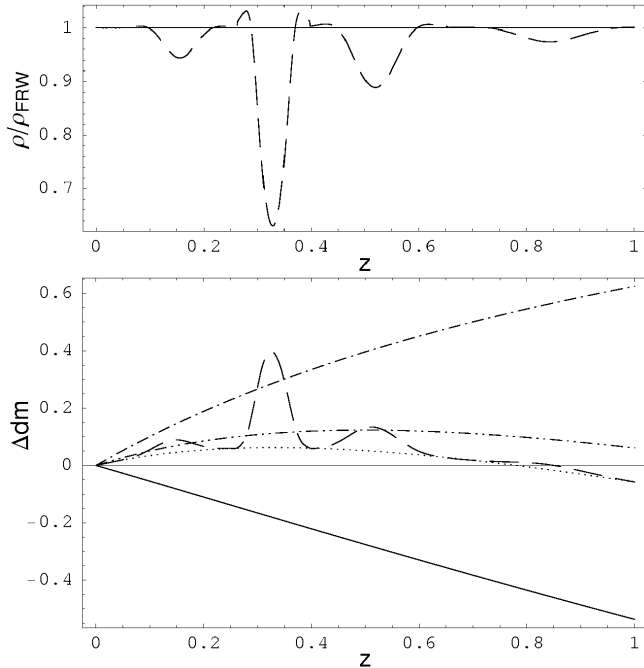


Figure 13. The same as Figure 11, but with the deeper void distribution, with $\sim 68\%$ of void $< 25\%$ under-dense.

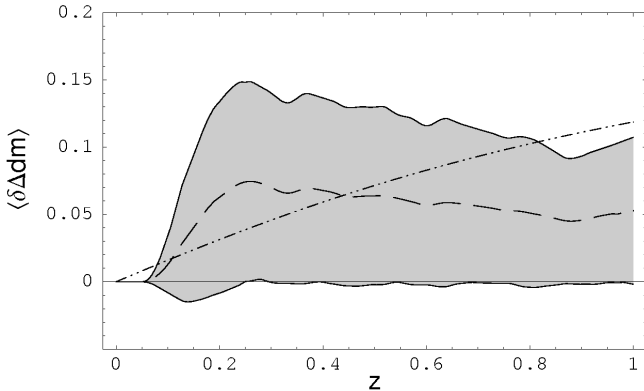


Figure 14. The same as Figure 12, but with the deeper void distribution, with $\sim 68\%$ of void $< 25\%$ under-dense.

them. Of course, we will also be interested in what these results imply for more realistic situations. To address this we will take simulations of what real density fields in the Universe are believed to look like. These density fields will then be idealised so as to appear as Swiss Cheese: Over-dense regions will be taken as FRW cheese, and under-dense regions will be modelled as LTB holes (with the appropriate width and depth). The real Universe, of course, is not an exact Swiss Cheese, and so our idealisation will require some considerable approximation. Our aim in this section is not to determine precisely what an observer in these space-times should see, but to obtain better motivated Swiss Cheese models, derived from realistic simulations, rather than from idealised distributions. One would hope that results derived in this way would be more indicative of what may be expected in the real Universe.

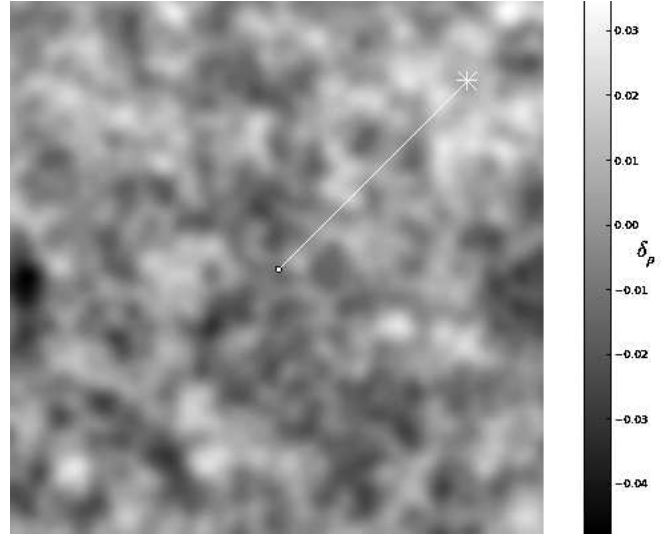


Figure 15. A slice through a simulation of linear structure generated from a Λ CDM power spectrum. The field is approximately 1200 Mpc across today, corresponding to a radius in redshift of ~ 0.15 . An example line of sight to a supernova is shown.

5.1 Density Fields

Extracting real density profiles from redshift surveys in the face of limited survey regions, and redshift-space distortions, is somewhat complex (Fisher et al. 1995; Erdogdu 2004). In addition, the formalism we have used up to this point takes density along a space-like projection of a line of sight into a surface of constant t , whereas real observations are made along past light cones. We will therefore use simulations of linear and non-linear structure formation to generate line-of-sight profiles of the energy density. These simulations all have $\Omega_\Lambda = 0.7$ in their backgrounds.

5.1.1 Linear Structure

In the linear regime we can use the realisation of a power spectrum to create a three-dimensional density field. We use the Boltzmann code CAMB⁴ (Lewis et al. 2000) to generate a dark matter power spectrum $\Delta_k^2 = \langle \delta_k^* \delta_k \rangle$ at $z = 0$ from the WMAP 5-year best-fit concordance cosmological parameters. The Fourier-domain density field is then a 3D Gaussian random-phase realisation of such a power spectrum with the symmetries that generate a real-space density map with no imaginary component. The scale and resolution of the simulation are determined by the minimum and maximum wavenumbers used; we use values to generate results roughly comparable to the Millennium regime (see below). A space-like slice through this space-time is shown in Figure 15.

5.1.2 Non-Linear Structure

As a simulation of non-linear structure we use the results of the Millennium N-body Simulation (Lemson et al. 2006; Springel 2006). The Millennium Simulation modelled a cubic region of space with a side length of $500/h$ Mpc, where $h \equiv$

⁴ <http://camb.info>

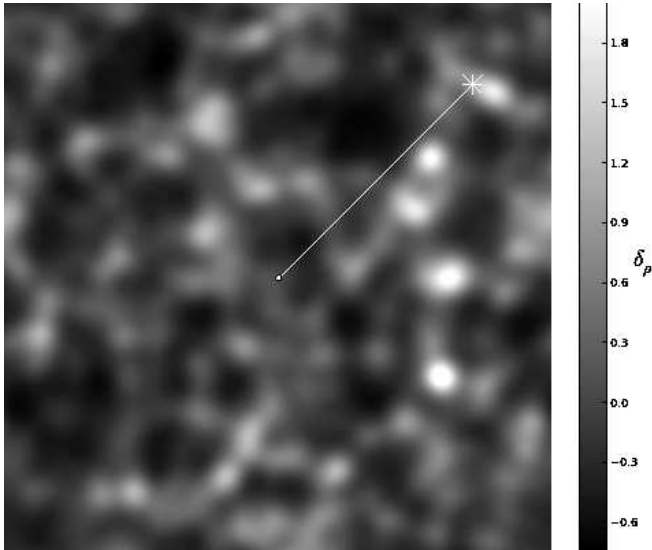


Figure 16. A slice through the Millennium Simulation, smoothed on scales of 10Mpc. The field is 715 Mpc across, the full size of the simulation. An example line of sight to a supernova is shown.

$H_0/100 \text{ km s}^{-1} \text{ Mpc}^{-1} = 0.7$. It modelled 10^{10} dark matter particles in 256^3 cells with periodic boundary conditions, which for our purposes are especially suitable for smoothing on new scales. The database for the simulation⁵ directly stores densities smoothed on various scales from 1.25Mpc to 10.0Mpc.

5.1.3 Smoothing Scales

The size of density fluctuations is determined, at least in part, by the smoothing scale applied to the data (the radius of the Gaussian kernel convolved with the data), or, equivalently, to the resolution at which a realisation is generated. Since the linear approximation to structure is only valid on large scales, our linear realisations are already beyond the domain of this problem, but our choice of smoothing scale for the non-linear simulation is critical. On small smoothing scales fluctuations are very large, but in these regimes the pressureless dust approximation of the LTB model could break down. In addition, on very small scales discrete particles (i.e. galaxies) may become resolvable, and the fluid approximation itself could then be in question. However, if we choose the smoothing scale to be too large then we will under-estimate the density fluctuations, and hence the effect on the distance modulus. We use smoothing scales of 10 and 20 Mpc; the former is direct from the Millenium database and the latter is manually smoothed with a Gaussian filter. Slices through the smoothed Millennium Simulation are shown in Figures 16 and 17. The former has a smoothing scale of 10Mpc, and the latter is the same density field with a smoothing scale of 20Mpc.

5.2 Distance Moduli

In both linear and non-linear density fields, lines of sight are taken in random directions from the centre of the simulation.

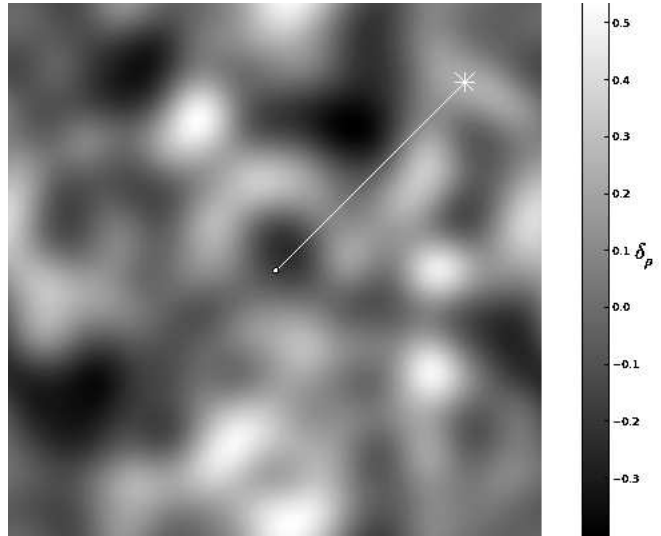


Figure 17. The same Millennium Simulation slice as in Figure 16, but smoothed on 20Mpc scales.

We then convert the density profiles along these lines into sets of voids that can be used as input for the formalism developed above. We approximate any under-dense segments of the line as being produced by a void generated from a Gaussian perturbation in the curvature, k , with the same depth and width as the segment. If an under-dense region is split into two by a local maximum that is less than half the depth of its shallowest neighbouring minima, then such an under-density is considered as two voids back to back. Over-dense regions are simply replaced by FRW geometry, with the same density as the background. We also ignore the effect of the local void that, coincidentally, happens to lie at the centre of the Millenium Simulation. As mentioned above, local voids have a different effect to the distant voids we are concerned with here.

5.2.1 Linear Structure

Figure 18 shows the density profile along the example line of sight (as shown in Figure 15), the corresponding Swiss Cheese density profile, and the consequent distance modulus. The under-densities in the upper panel of this figure can be seen to be very small, with a depth of order $\sim 1\%$, as would be expected from a linearly perturbed density field. The voids in the idealised Swiss Cheese density profile appear slightly narrower than the under-densities in the smoothed energy density distribution. This is due to the width of the k perturbation being fitted to smoothed under-density, and not to the width of the perturbation in ρ (it is k that is most directly related to the perturbation in Δ_{dm}). The lower panel of Figure 18 shows that the effect of such modest structures on the distance modulus is minor, though clearly non-zero.

Taking 1000 lines of sight, all starting from the same point in our density field, we can now estimate the magnitude of the displacement, and dispersion, one may expect from the background distance modulus if one were to make observations of supernovae over many different directions on the sky. The resulting mean displacement from the background value, and standard deviation about this mean, are

⁵ <http://www.mpa-garching.mpg.de/millennium/>

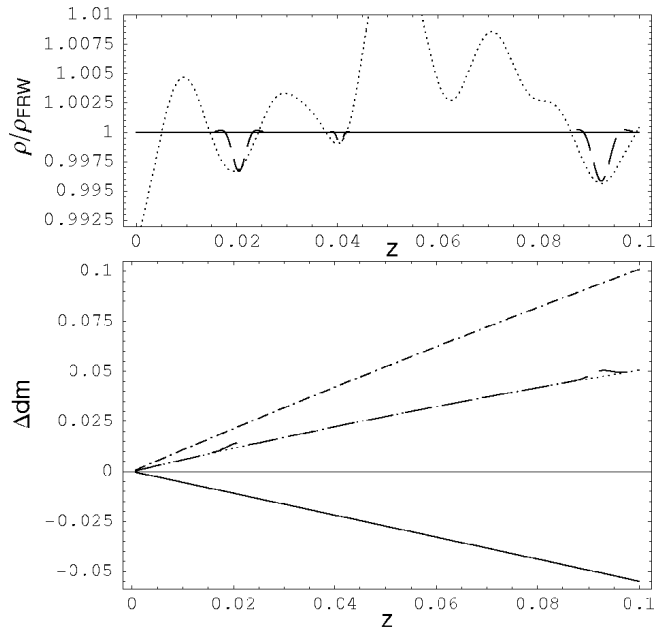


Figure 18. The upper panel shows the density along the line of sight path shown in Figure 15 as the dotted line, and the energy density of our idealised Swiss Cheese as the dashed line. The lower panel shows the distance modulus generated by Swiss Cheese as the dashed line.

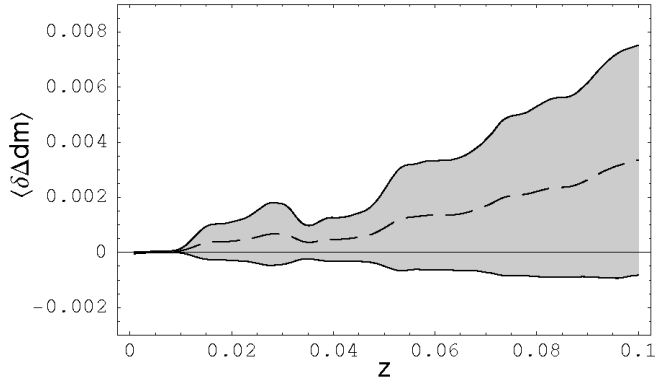


Figure 19. The same as Figure 8, but for the linear structure simulation.

shown in Figure 19. In keeping with the shallowness of the voids, the mean displacement and dispersion in this figure can be seen to be very small. Unlike the corresponding plots in Section 4, the mean deviation in Figure 19 does not flatten out. This is due to correlations in the location of voids in the density field of Figure 15. Such correlations were absent in the randomly distributed voids used previously.

5.2.2 Non-Linear Structure

Now let us consider the non-linear density fields obtained from smoothing the 10^{10} particles of the Millennium Simulation on different scales. We will begin by considering a smoothing scale of 10Mpc. In this case, the density profile along the example line of sight from Figure 16 is shown in Figure 20. The voids here can be seen to be an order of magnitude deeper than those of the linearly perturbed density field shown in Figure 18, above. Correspondingly, the per-

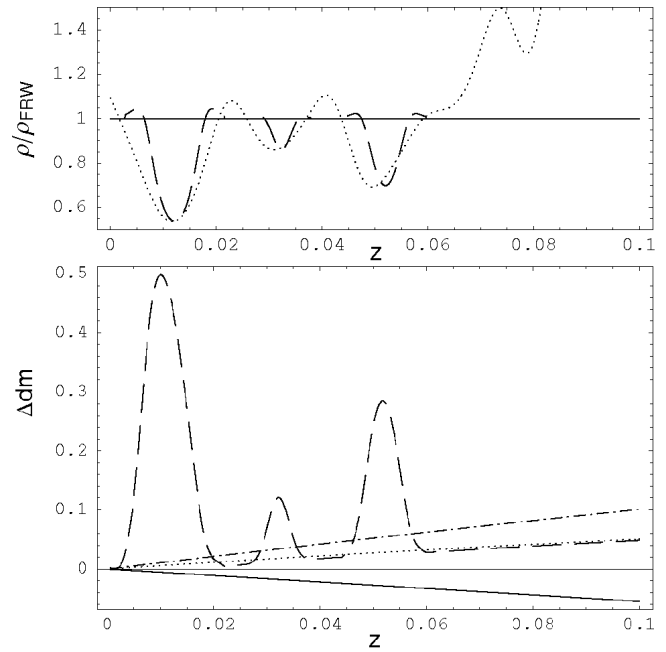


Figure 20. The density profile from the example line of sight shown in Figure 16, the fitted Swiss Cheese density profile, and the resulting distance modulus. All lines as in Figure 18, but now for the Millennium Simulation smoothed on 10Mpc scales.

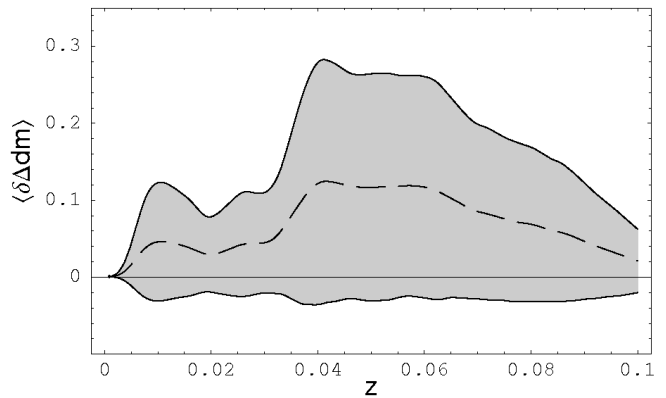


Figure 21. The same as Figure 19, but for the Millennium Simulation smoothed on 10Mpc scales.

turbation in distance modulus is also an order of magnitude larger.

The mean displacement in distance modulus, and standard deviation about that mean, are shown in Figure 21 for a sample of 1000 lines of sight. These values are more than an order of magnitude larger than those of the linearly perturbed density field, and are now comparable to the difference in distance modulus between a spatially flat, dust dominated EdS universe, and Λ CDM with $\Omega_\Lambda = 0.7$.

As mentioned above, the results we obtain in this section are strongly dependent on the chosen scale of smoothing. Of course, in reality there is only one local expansion rate of space at any given point, but without any knowledge of the smoothing scale to which this corresponds it seems most prudent for us to illustrate the effect of choosing different scales. To this end, we will now consider the results obtained from smoothing on a scale of 20Mpc. In this case

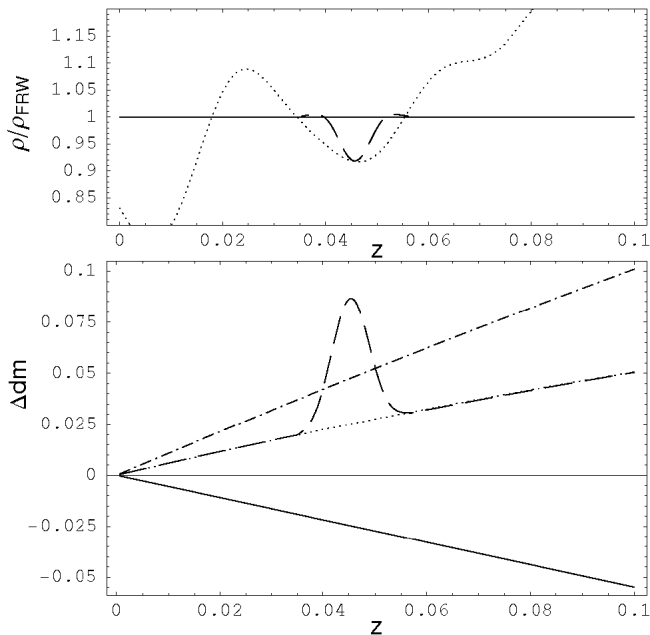


Figure 22. The same line-of-sight density profile, fitted voids, and distance modulus plots as in Figure 18, but for the Millennium Simulation smoothed on 20Mpc scales.

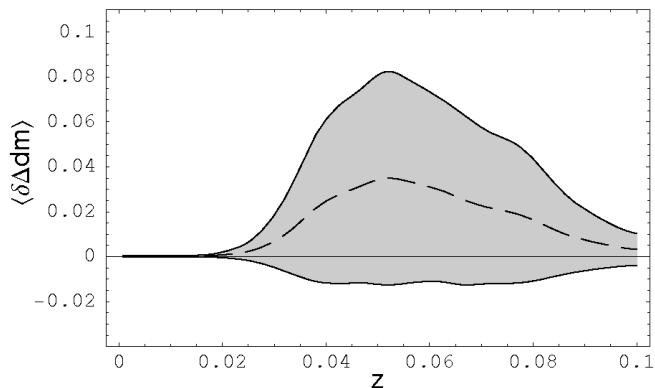


Figure 23. The same as Figure 19, but for the Millennium Simulation smoothed on 20Mpc scales.

the density profile along the example line of sight from Figure 17 is shown in Figure 22, together with the corresponding distance modulus plot.

The mean and standard deviation of the difference in distance modulus from the background value, for 1000 lines of sight, are shown in Figure 23. This plot can be seen to be significantly different to Figure 21: Doubling the smoothing scale has more than halved the magnitude of the displacement and dispersion. Such strong dependence on the smoothing scale shows that understanding the spatial variation of local expansion rates in an inhomogeneous universe could be of critical importance in determining its Hubble diagram.

6 DISCUSSION

We have considered here the non-linear effects of large structures on Hubble diagrams. Using the spherically sym-

metric LTB solution of Einstein's equations we have constructed a Swiss Cheese model of the Universe. In this model the background space-time is taken to be a spatially flat FRW universe, filled with dust and a cosmological constant. Spherically symmetric regions of this background cosmology are then removed and replaced with the regions of negatively curved LTB space-time, matched appropriately at the boundary. The resulting cosmology has an initially evenly distributed energy density. The regions with negative spatial curvature then expand more quickly than the background, and large under-dense voids form. These voids behave like open FRW space-time at their centre and transition smoothly to over-dense regions at their edge, before matching onto the background. Such a universe is an exact inhomogeneous solution of Einstein's equations, with a simple enough geometry to allow explicit exact calculations of luminosity distances to be performed within it.

By considering the cross-sectional area of a bundle of radial null geodesics, focused on an observer in the background space-time, we are able to obtain a simple analytic expression for the angular diameter distances such an observer will infer for objects in, and beyond, the void. The luminosity distance then follows straightforwardly, and we can calculate the Hubble diagram that our observer will see along such a line of sight. The expressions derived are limited to spherically symmetric voids, and to lines of sight that look directly through their centres, but have the great benefit that they are exact. As such, all non-linear effects due to position dependent spatial curvature, expansion rates, and energy densities are automatically included.

We then consider the effect of a single large void on Hubble diagrams constructed by an observer looking through it. We find that observations of objects beyond the void are not noticeably affected by its presence. When viewing objects within the void, however, the effect of the voids presence can be of some size. We illustrate the differences witnessed by our observer by considering the distance modulus of a source, minus the magnitude it would have at the same redshift in an empty Milne universe. We consider voids with an even distribution of gravitational mass, and a Gaussian shaped under-density in spatial curvature. In this case the magnitude to an object in the void is made greater by the voids presence, so that the object appears dimmer on the sky. The maximum displacement from the background distance modulus appears proportionate to the fractional under-density at the centre of the void, and is largely insensitive to the presence of Λ . This can be seen from Figures 3 and 6, where the relation between void depth and distance modulus displacement can be seen to mildly super-linear. The effect of a non-zero Λ manifests itself principally in the suppression it causes in the growth of structure.

Having studied the case of a single void, we then move on to consider a universe containing many voids. In this case we draw the void widths and depths randomly from probability distributions. We consider a shallow distribution of voids, in which $\sim 68\%$ of voids are $< 10\%$ under-dense at their centre, and a deeper distribution, in which $\sim 68\%$ are $< 25\%$ under-dense. By generating 1000 sets of voids from each distribution, we produce a mean deviation from the background distance modulus, and the standard deviation that should be expected from that mean. As found

in the case of single voids, the displacement of the distance modulus from the background value is proportionate to the depth of voids considered. The dispersion is similarly dependent on typical void depth.

Using a linearly perturbed density profile, and data from the Millennium Simulation, we then proceed to consider how structures in more realistic universes could affect the Hubble diagrams constructed by observers in them. To achieve this we take a number of different lines of sight from a central position in the simulation. The density profile along these lines are determined, in the case of Millennium Simulation, by smoothing on different scales. We then treat under-densities as being formed from spherically symmetric, Gaussian perturbations in k , and calculate the distance moduli along lines of sight that pass through them. Over-densities are not modelled well in this formalism, and so any over-dense regions are simply replaced by regions of FRW space-time, with the background density and expansion rate.

The effects of the voids in the linearly perturbed space-time are small, but non-zero. Using the data from the Millennium Simulation, however, much deeper voids are realised. These voids can have a considerable effect on the Hubble diagrams constructed by observers in the space-time, and produce large deviations and dispersion in the distance modulus. The magnitude of this effect, however, is strongly dependent on the depth of voids, which is itself a function of how the smoothing from discrete sources, to continuous fluid is performed. Increasing the smoothing scale decreases the depth of void, and hence decreases the effect on the Hubble diagram. Ultimately, it appears that one needs to know the appropriate scale on which to smooth, if one wants to make reliable quantitative predictions. We do not attempt to solve this problem here, but point out that as long as there is a well defined local expansion rate at a point in space, then such a scale must surely exist.

We find the non-linear effects of inhomogeneity in the Universe can both displace the average distance modulus from its background value, and introduce dispersion around that average. These effects, if improperly accounted for in fitting data to FRW models, could lead to systematic errors in extracting cosmological parameters, and an under-estimation of the errors involved. Such an effect may be of use for accounting for some of the ‘intrinsic error’ usually added to supernovae data when fitting to cosmological models, and which is often a large fraction of the total error. We find that the the magnitude of these effects is most sensitive to the depths of voids involved.

The study we have performed here is limited in a number of respects, and rather than being exhaustive is instead intended to be a thorough investigation of the simplest case. One will certainly be interested in the effects introduced by different void profiles, rather than the simple Gaussian with constant gravitational mass considered here. It will also be of much interest to determine the effects of looking through voids in an off-centre way. It was suggested by Vanderveld, Flanagan & Wasserman (2008) that such observations can be considerably different to observations directly through the centre. Generalising the present study to off-centre observations is not trivial, but is certainly possible, and will be considered elsewhere. There are also issues of bias that one may wish to take into account in more detailed studies. For instance, it may be the case that more

supernovae occur in denser regions of the Universe, or that supernovae in less dense regions are easier to observe.

This study could be further generalised by considering non-spherical voids, and by better accounting for over-dense regions of the Universe. The LTB voids considered here are only solutions as long as pressure is negligible. A similar study including anything approaching a realistic over-density will therefore require solutions with more general fluid content, which are considerably more difficult to find. It is feasible that the inclusion of over-densities in a more satisfactory way could cancel some of the displacement effect, but it is hard to see how it could counteract the dispersion. In Appendix B we consider the effect of having spherically symmetric shells of under-density, rather than spherical holes (an Onion universe, rather than Swiss Cheese). In this case the effects of the under-densities produce deviations in the distance modulus with the same order of magnitude, but with the opposite sign, to Swiss Cheese. This shows that a full understanding of the way that large scale structure effects Hubble diagrams is likely to be a complicated function of the detailed geometry of the inhomogeneous Universe.

Finally, one may speculate on the effects of large scale structure as potentially mitigating the need for Dark Energy. We find that the voids required to mistake an Einstein-de Sitter background for Λ CDM with $\Omega_\Lambda = 0.7$ would have to be very deep. Even the void distribution considered in Figure 10 does not come close (although the Millennium Simulation smoothed on small enough scales may do). The voids involved would likely have to be more than 50% under-dense at their centre. Even if such voids did exist, their ability to mimic the shape of the distance modulus of Λ CDM would rely on some fortuitous correlations in their positions, so that the mean Δm peaks at around $z \sim 0.5$ and drops off at lower redshifts. Alternatively, one may consider extending the present study so that the background Cheese is spatially curved, or so that we are at the centre of a void. The effects of a local void have been shown by a number of authors to be able to mimic, at least to some degree, the presence of Λ on the Hubble diagram (Alexander, Biswas & Notari 2007; Alnes, Amarzguoui & Grøn; Garcia-Bellido & Haugboelle 2008; Clifton, Ferreira & Land 2008; Bolejko & Wyithe 2008), but requires a very deep and wide structure. It seems conceivable that the effects uncovered here could be combined with the effects of living at the centre of a void, so that the demands on the depth and width of our local void could be somewhat relaxed. We will not speculate on this any further here.

ACKNOWLEDGEMENTS

We are grateful to C. Clarkson, P. Ferreira and J. Silk for helpful suggestions and discussion. TC acknowledges the support of Jesus College, and JZ acknowledges that of the STFC. We are also grateful to have received support from the BIPAC.

REFERENCES

- Hogg D. W. et al., 2005, *ApJ*, 624, 54.
- Labini F. S. et al., 2008, *arXiv:0805.1132* [astro-ph].

- Watkins R., Feldman H. A., Hudson M. J., 2008, arXiv:0809.4041 [astro-ph].
- Land K., Magueijo J., 2005, PRL, 95, 071301.
- Inoue K. T., Silk J., 2006, ApJ, 648, 23.
- Dyer C. C., Roeder, R. C., 1972, ApJ, 174, L115.
- Dyer C. C., Roeder R. C., 1973, ApJ, 180, L31.
- Dyer C. C., Roeder R. C., 1974, ApJ 189, 167..
- Sasaki M., 1987, MNRAS, 228, 653.
- Futamase T., Sasaki M., 1989, PRD, 40, 2502.
- Kasai M., Futamase T., Takahara F., 1990, Phys. Lett. A, 147, 97.
- Kantowski R., 1998, ApJ, 507, 483.
- Sugiura N., Sugiyama N., Sasaki M., 1999, Prog. Theo. Phys., 101, 903.
- Pyne T., Birkinshaw M., 2004, MNRAS, 348, 581.
- Bonvin C., Durrer R., Alice Gasparini M., 2006, PRD, 73, 023523.
- Lemaître G., 1933, Ann. Soc. Sci. Brussels, A53, 51.
- Tolman R. C., 1934, Proc. Nat. Acad. Sci. USA, 20, 169.
- Bondi H., 1947, MNRAS, 107, 410.
- Zecca A., 1991, Nouvo Cim., B106, 413.
- Biswas T., Notari A., 2008, JCAP 06, 021.
- Marra V. et al., 2007, PRD, 76, 123004.
- Bonnor W. B., Vickers P. A., 1981, Gen. Rel. Grav., 13, 29.
- Ribeiro M. B., 1992, ApJ, 388, 1.
- Sachs R., 1961, Proc. Roy. Soc. A, 264, 309.
- Etherington I. M. H., 1933, Phil. Mag., 15, 761.
- Bonnor W. B., 1974, MNRAS, 167, 55.
- Alexander S., Biswas T., Notari, A., 2007, arXiv: 0712.0370 [astro-ph].
- Alnes H., Amarzguoui M., Grøn Ø., 2006, PRD, 73, 083519.
- Garcia-Bellido J., Haugboelle T., 2008, JCAP, 04, 003.
- Clifton T., Ferreira P. G., Land K., 2008, PRL, 101, 131302.
- Bolejko K., Wyithe J. S. B., 2008, arXiv:0807.2891 [astro-ph].
- Fisher K. et al., 1995, MNRAS, 272, 885.
- Erdogdu P. et al., 2004, MNRAS, 352, 939.
- Lewis A. et al., 2000, ApJ, 538, 473.
- Lemson G. and the Virgo Consortium, 2006, astro-ph/0608019.
- Springel V. et al., 2005, Nature, 435, 629.
- Vanderveld R. A., Flanagan E. E., Wasserman I., 2008, PRD, 78, 083511.

APPENDIX A: SOLID ANGLE

Consider a non-radial geodesic with tangent vector \tilde{k}^a , in a direction \tilde{n}^a in the rest space of a co-moving observer with 4-velocity u^a . Coordinates can be chosen such that this geodesic is confined to the plane $\theta = \pi/2$. In this case, the ϕ independence of (1) allows the integral of the Euler-Lagrange equations

$$\frac{d\phi}{d\tilde{\lambda}} = \frac{J}{R^2}, \quad (\text{A1})$$

where J is a constant that parameterises the geodesic. Now, if \tilde{n}^a is a unit vector in a plane tangent to u^a , then $\tilde{n}^a \tilde{n}_a = 1$ and $\tilde{n}^a u_a = 0$, so that

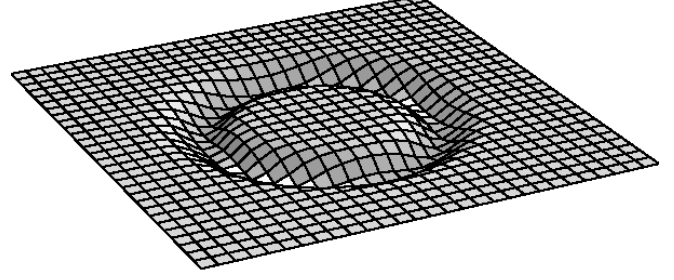


Figure B1. An illustration of $k(\mathbf{x})$ in an Onion universe. The surface displayed is a constant time slice, with one spatial dimension suppressed. Vertical displacement indicates a fluctuation in k , and distance from the centre is proportional to comoving distance, r .

$$\tilde{n}^a = \frac{1}{\tilde{A}} \left(0, \tilde{v}_r, 0, \frac{J}{R^2} \right), \quad (\text{A2})$$

where $\tilde{A} \equiv dt/d\tilde{\lambda}$ and $\tilde{v}_r \equiv dr/d\tilde{\lambda}$. The constraint equation can then be read off (1), as

$$-\left(\frac{dt}{d\tilde{\lambda}}\right)^2 + \frac{R'^2}{(1-kr^2)} \left(\frac{dr}{d\tilde{\lambda}}\right)^2 + \frac{J^2}{R^2} = 0, \quad (\text{A3})$$

and the angle measured in the rest space of a co-moving observer at r between this geodesic and a radial one is

$$\cos \psi = g_{ab} \tilde{n}^a \tilde{n}^b = \frac{\tilde{v}_r}{\tilde{A}} \frac{R'}{\sqrt{1-kr^2}} = \sqrt{1 - \frac{J^2}{\tilde{A}^2 R^2}} \quad (\text{A4})$$

or

$$\sin \psi = \frac{J}{\tilde{A} R}, \quad (\text{A5})$$

where (A3) has been used in the last line of (A4). Rotational symmetry then allows us to infer the solid angle subtended by a set of rays parameterised by J , focused at a point r , and centred about a radial geodesic, to be

$$d\Omega = \frac{J^2}{\tilde{A}^2 R^2}. \quad (\text{A6})$$

APPENDIX B: AN ONION UNIVERSE

As an alternative to considering the Swiss Cheese model, one can also use the LTB solution to consider an ‘Onion universe’, in which there are under-dense shells of matter in a spherically symmetric space-time. Although less appealing as a way of modelling the real inhomogeneous Universe, a brief consideration of luminosity distances in such a space-time will allow us to put the Swiss Cheese results in some context. In the Onion universe the requirement of lines of sight passing through the centre of spherical under-densities is removed, while the problem can still be treated in an exact way. An example of the spatial curvature profile of an Onion universe is given in Figure B1, where a surface of constant time is shown, with one spatial dimension suppressed. Vertical displacement indicates a fluctuation in k , and distance from the centre is proportional to comoving distance, r .

The observer in this space-time is taken to be at the centre of symmetry, so that the luminosity distance to a source at (t_e, r_e) is given by (25). In Figure B2 we show a couple of example cases. The radial profile of the curvature perturbation in each of these cases is that of a Gaussian,

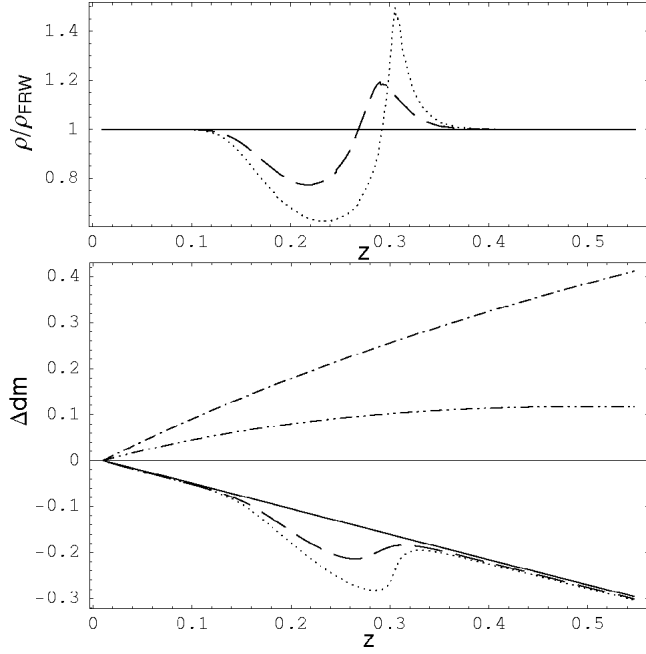


Figure B2. The upper panel shows two example density profiles resulting from Gaussian perturbations in $k(r)$, with different depths. The lower panel shows the corresponding distance moduli. The dot-dashed, double-dot-dashed and solid lines are as in Figure 1.

with its minimum displaced from the centre of symmetry. The upper panel in Figure B2 shows the energy density, as a function of redshift, experienced by the photon as it travels along our past light cone. While the perturbation in $k(r)$ is symmetric, being a Gaussian, the resulting energy density distribution can be seen to be highly asymmetric, with a considerable over-density on the side of the under-dense shell that is furthest from the observer.

In the lower panel of Figure B2 we plot the distance modulus that would be measured by an observer at the centre of symmetry, for these two different cases. It can be seen that the under-density produces a considerable deviation from the background EdS model. Comparing this effect with that shown in Figure 1, for the Swiss Cheese case, one can see that the magnitude of the deviation is $\sim 1/2$ as large. More striking, however, is that the under-density in the Onion universe causes a deviation in the *opposite* direction: Objects at the same redshift now appear brighter, rather than fainter.